Supplementary Information

Continuous-Flow Chemo-Enzymatic Gram-Scale Synthesis of Indole-3-Acetic Acid

Sippakorn Mapinta,[a] Sirus Kongjaroon [a], Duangthip Trisrivirat [a], Chatchai Kesornpun, [b] Jie Wu [c], Pimchai Chaiyen, [a] and Nopphon Weeranoppanant * [a, d]

[a] School of Biomolecular Science and Engineering, Vidyasirimedhi Institute of Science and Technology (VISTEC), Wangchan Valley, Rayong, 21210, Thailand.
[b] Future Biomanufacturing Research Hub (FBRH), Manchester Institute of Biotechnology, Department of Chemistry, The University of Manchester, Manchester M1 7DN, United Kingdom.
[c] Department of Chemistry, National University of Singapore, 3 Science Drive 3, 117543, Republic of Singapore
[d] Department of Chemical Engineering, Faculty of Engineering, Burapha University, Chonburi 20131, Thailand.
*Corresponding email: Nopphon.we@eng.buu.ac.th,

S1. Loading efficiency and relative activities using different immobilization condition

A

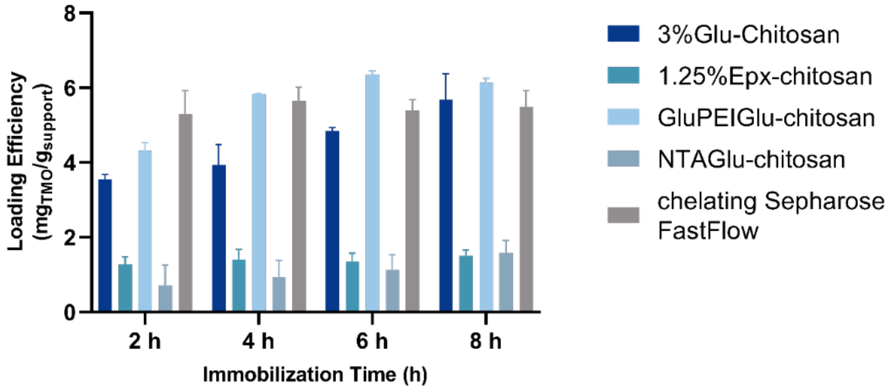

B

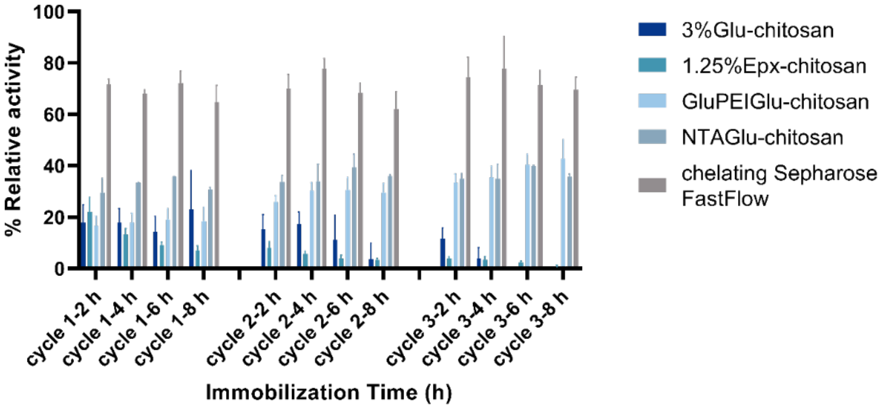

Fig. S1. (A) The loading efficiency when the TMO was immobilized using different tmmobilization times (2, 4, 6, 8 h) and different immobilization techniques (3% Glu-Chitosan or Glu, 1.25%Epx-Chitosan or Epx, GluPEIGlu-Chitosan or Glu@PEI@Glu, NTAGlu-Chitosan or Glu@NTA-Ni^{+2}, and chelating Sepharose™ Fast Flow). (B) The percentage of relative activity of the five methods from each immobilization time for 3 cycles.

S2. Adsorption test of L-Trp, IAM, IAA onto the Glu@PEI@Glu-chitosan

L-Trp, IAM, and IAA were tested for the physical adsorption over multiple cycles of reuse. All three chemical species exhibited significant physical adsorption when Glu@PEI@Glu resins were used, making these resins undesirable for the enzymatic reaction.

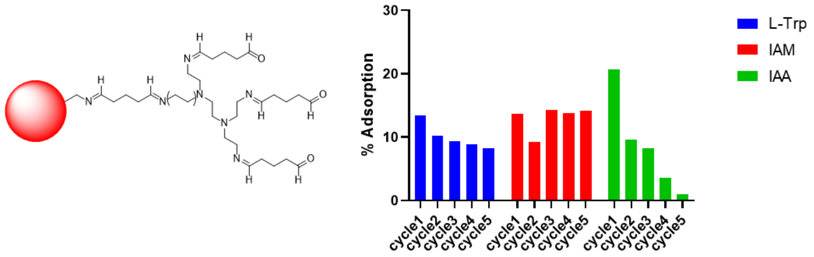

$$\% \, Adsorption = \frac{initial\ conc. - final\ conc.}{initial\ conc.} x\ 100$$

Fig. S2. The percent adsorption of L-Trp, IAM, and IAA onto the Glu@PEI@Glu resins

S3. Extent of hydrolysis using alkaline and acidic conditions

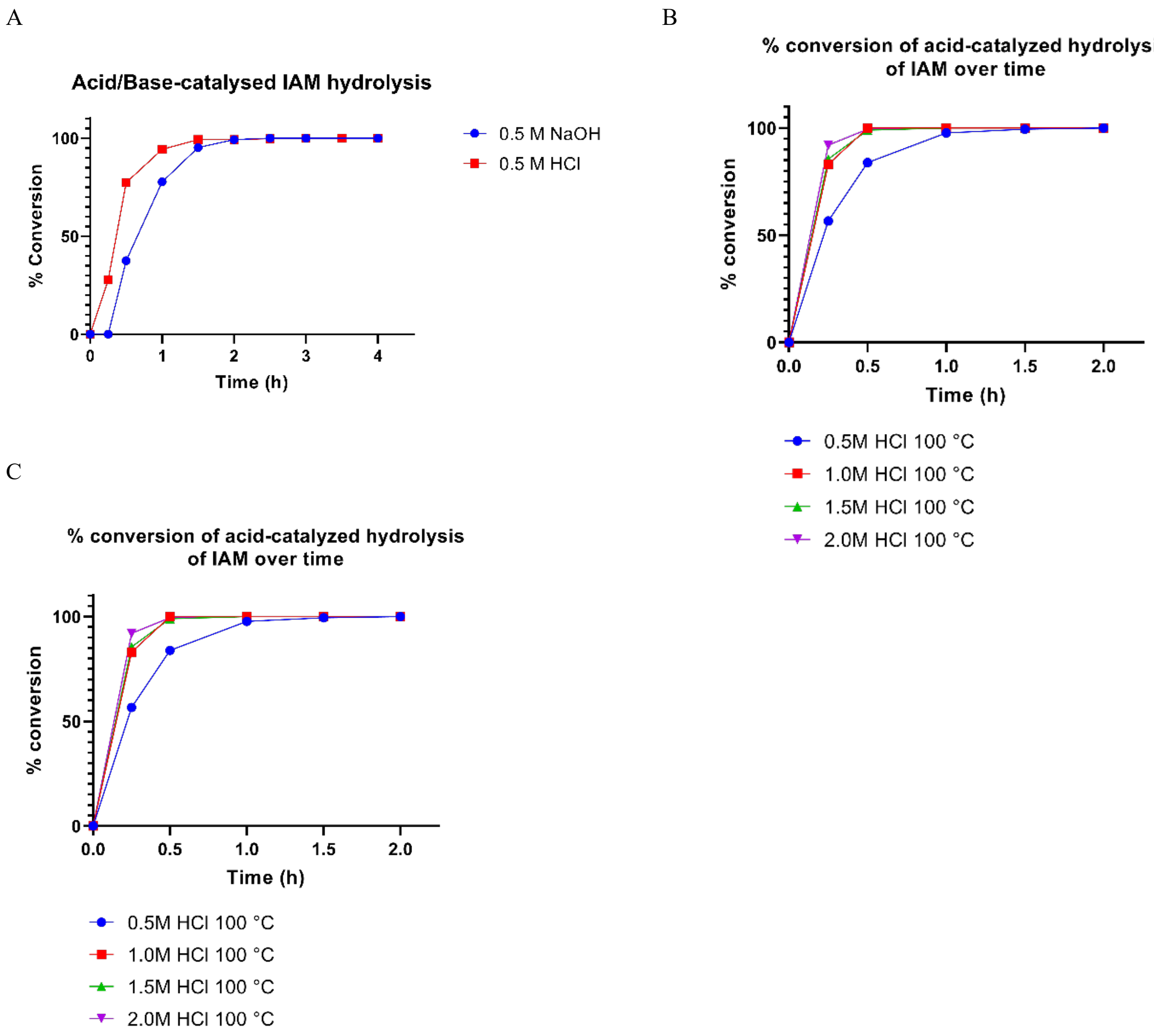

Fig. S3. (A) The percentage of IAM conversion catalyzed by HCl and NaOH, (B) the percentage of IAM conversion in base-catalyzed hydrolysis, (C) the percentage of IAM conversion in acid-catalyzed hydrolysis

S4. Proposed mechanisms of the IAM hydrolysis

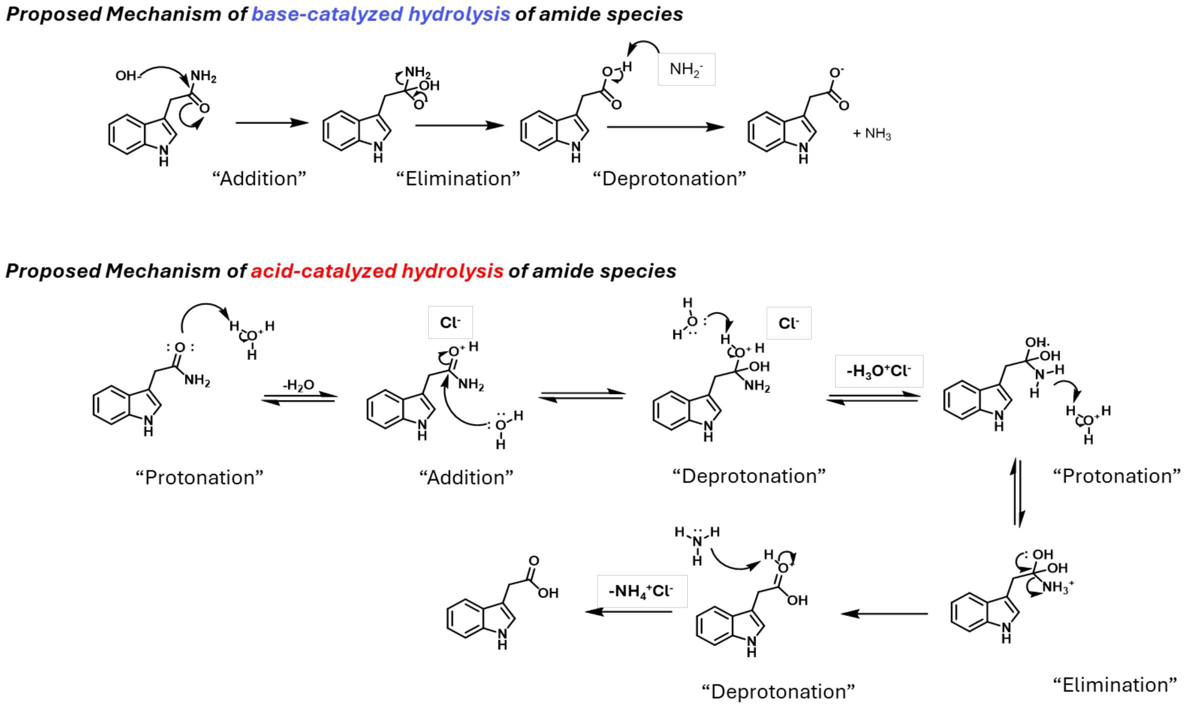

Proposed Mechanism of base-catalyzed hydrolysis of amide species

Proposed Mechanism of acid-catalyzed hydrolysis of amide species

Fig. S4. The proposed mechanisms of hydrolysis of the amide species using base and acid as catalysts.

S5. Degradation of IAA over different hydrolysis reaction temperatures

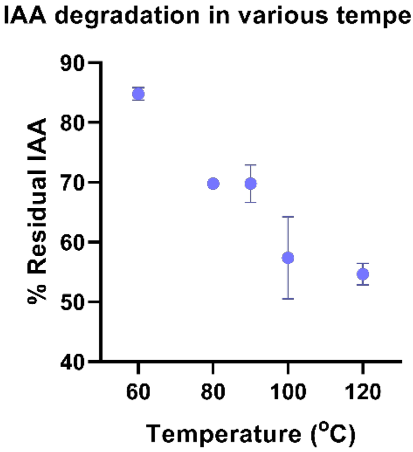

Fig. S5. The IAA degradation at various temperatures; the reaction was performed under the same condition as IAM hydrolysis for 30 min.

S6. Kinetic parameter estimation for the hydrolysis of IAM and the degradation of IAA at 80 ˚C

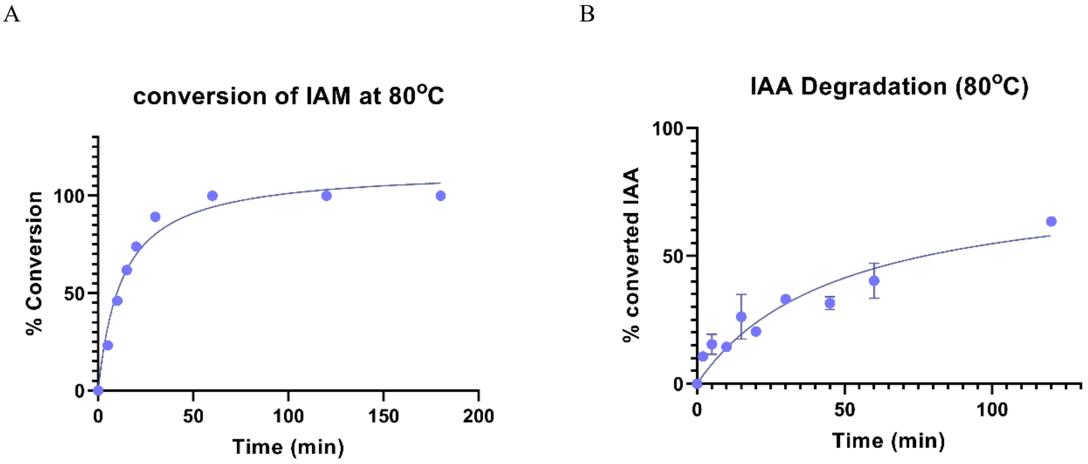

Reaction	Rate constant (s^{-1})
IAM conversion (k_1)	9.18×10^{-4}
IAA degradation (k_2)	$2.42 \quad 10^{-4}$

Fig S6. (A) The rate of IAM conversion fitted with GraphPad Prism to estimate the $t_{1/2}$, and k, (B) The rate of IAA conversion fitted with GraphPad Prism to estimate the $t_{1/2}$, and k.

S7. Analytical data of compounds obtained from the enzymatic reaction unit (first reactive step)

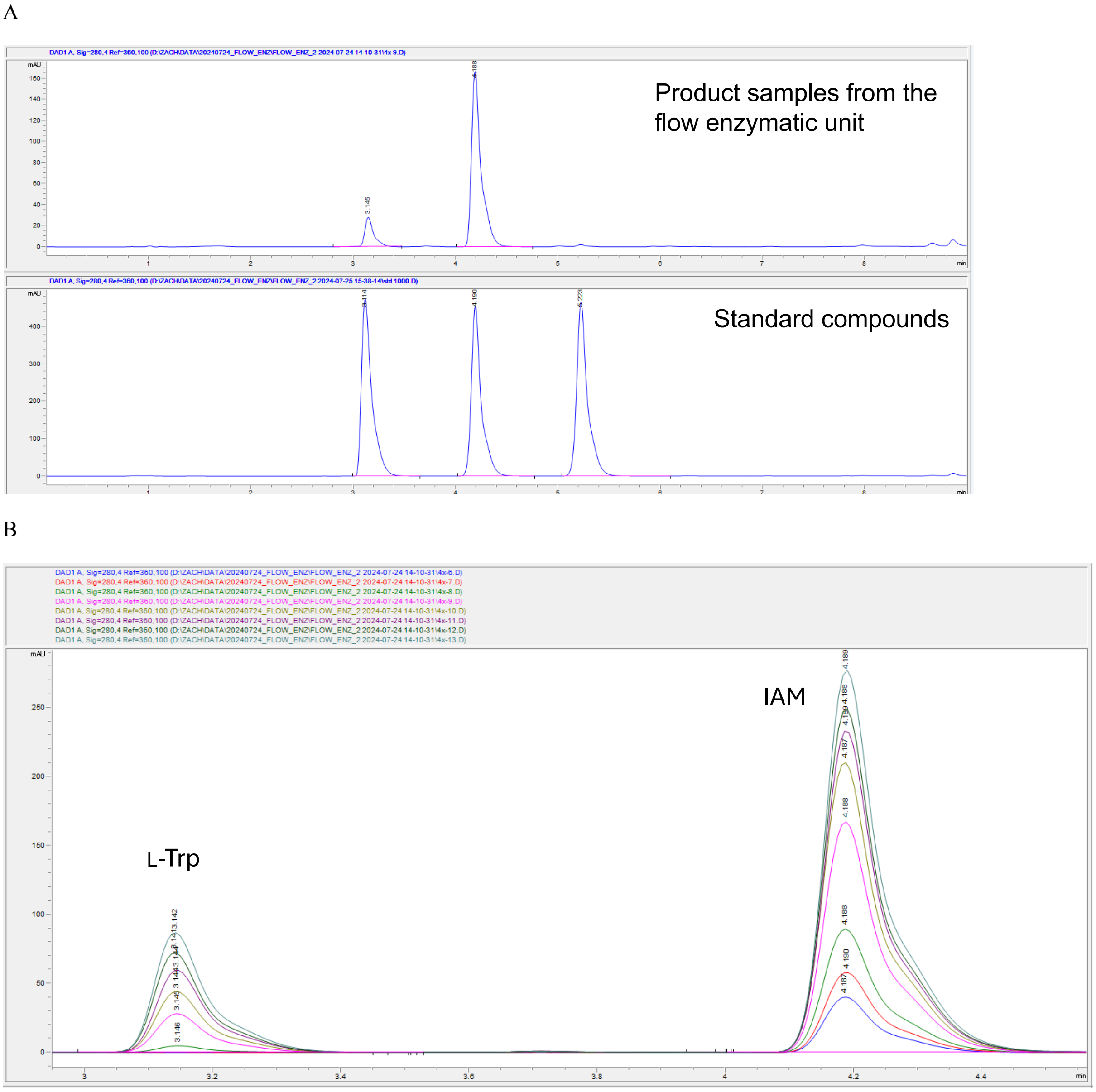

Fig S7.1 (A) HPLC-DAD Chromatogram of the product sample from the flow enzymatic unit and standard compound solutions, analyzed concurrently for compound identification verification. (B) HPLC-DAD chromatograms of product samples from the enzymatic reaction at various time points (4-15 h), illustrating the changes in product and substrate concentrations throughout the reaction.

A

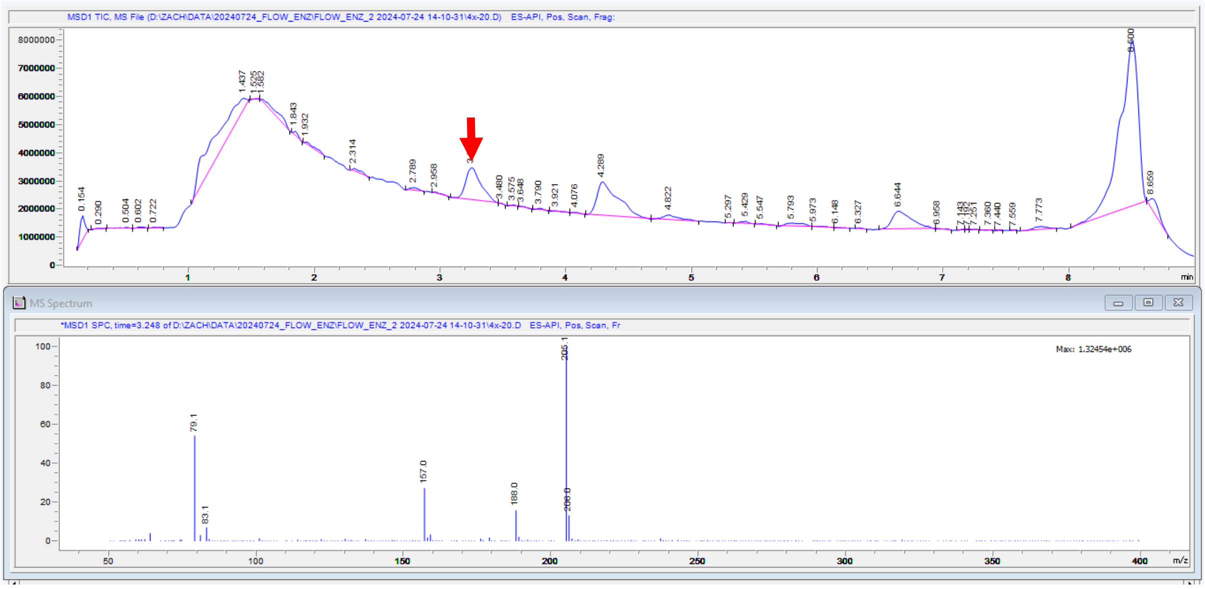

B

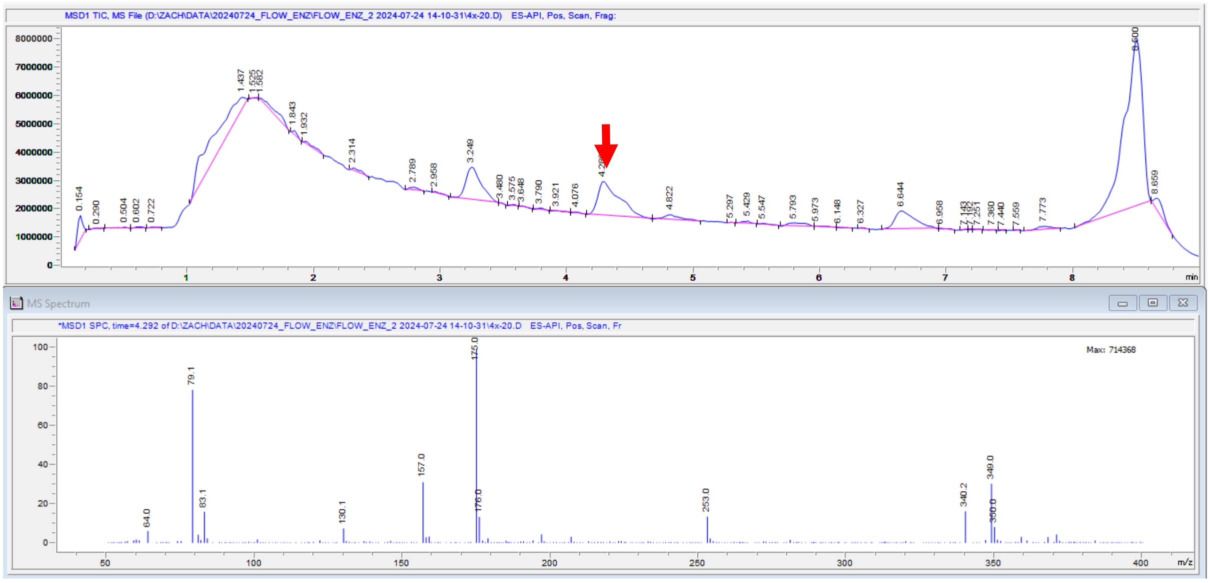

Fig S7.2 ESI-MS fingerprint of the product sample obtained from the flow enzymatic unit, as to confirm the identities of the L-Trp and IAM. (A) MS fingerprint of L-Trp (m/z of 205.1 (*M+1* ion peak), 206.0 (*M+1* isotopic peak)), (B) MS fingerprint of IAM (m/z of 175.0 (*M+1* ion peak), 176.0 (*M+1* isotopic peak)).

S8. Analytical data of compounds obtained from the hydrolysis unit (second reactive step)

A

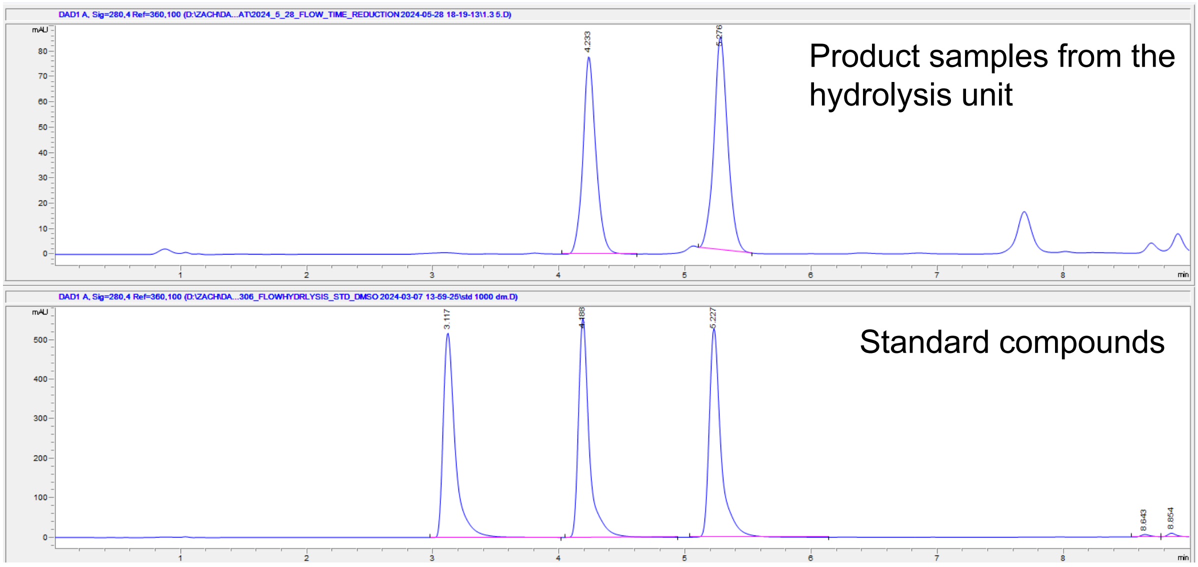

B

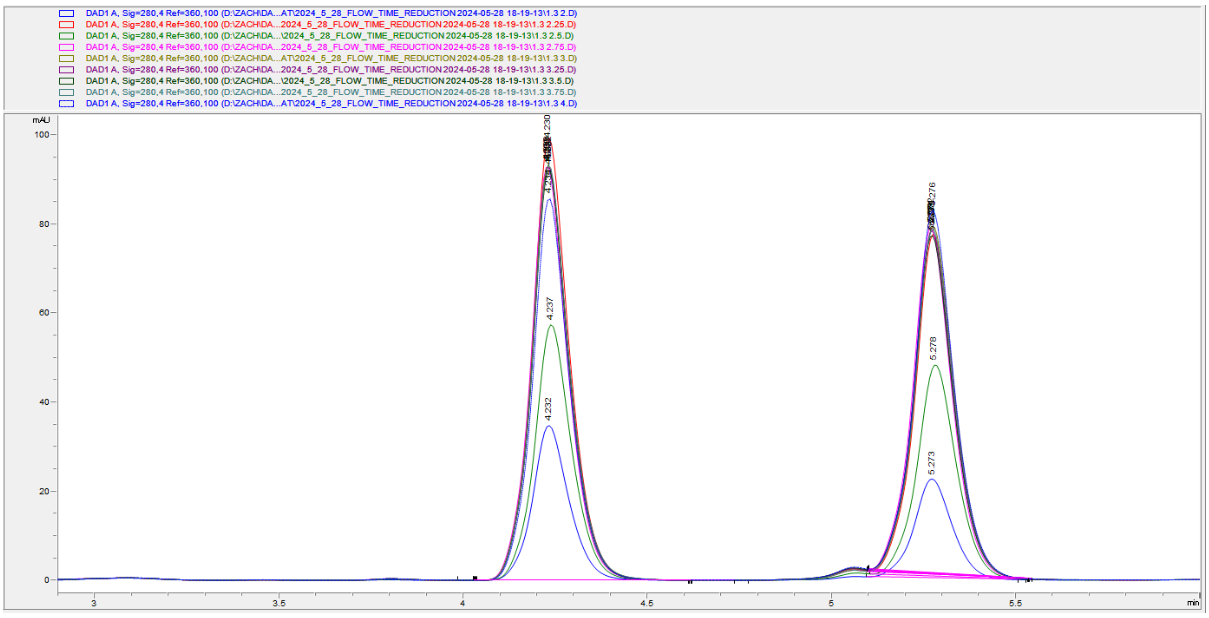

Fig. S8.1 (A) HPLC-DAD Chromatogram of the product sample from the hydrolysis unit and standard compound solutions, analyzed concurrently for compound identification verification. (B) HPLC-DAD chromatograms of product samples from the enzymatic reaction at different residence times (2 – 4 h), illustrating the changes in product and substrate concentrations throughout the reaction.

A

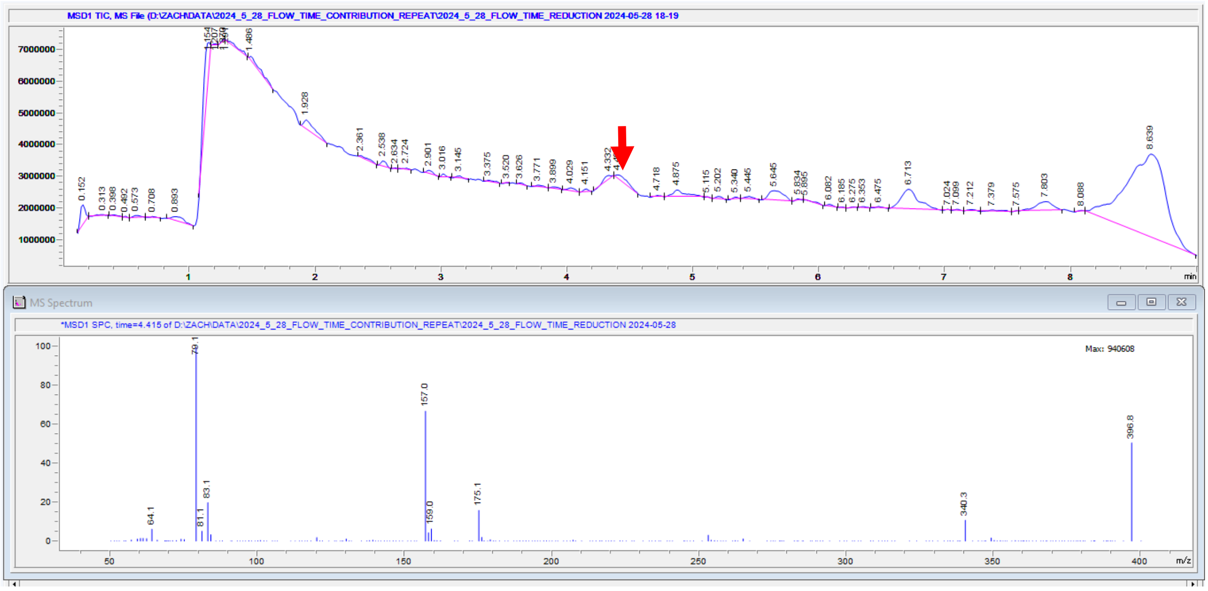

B

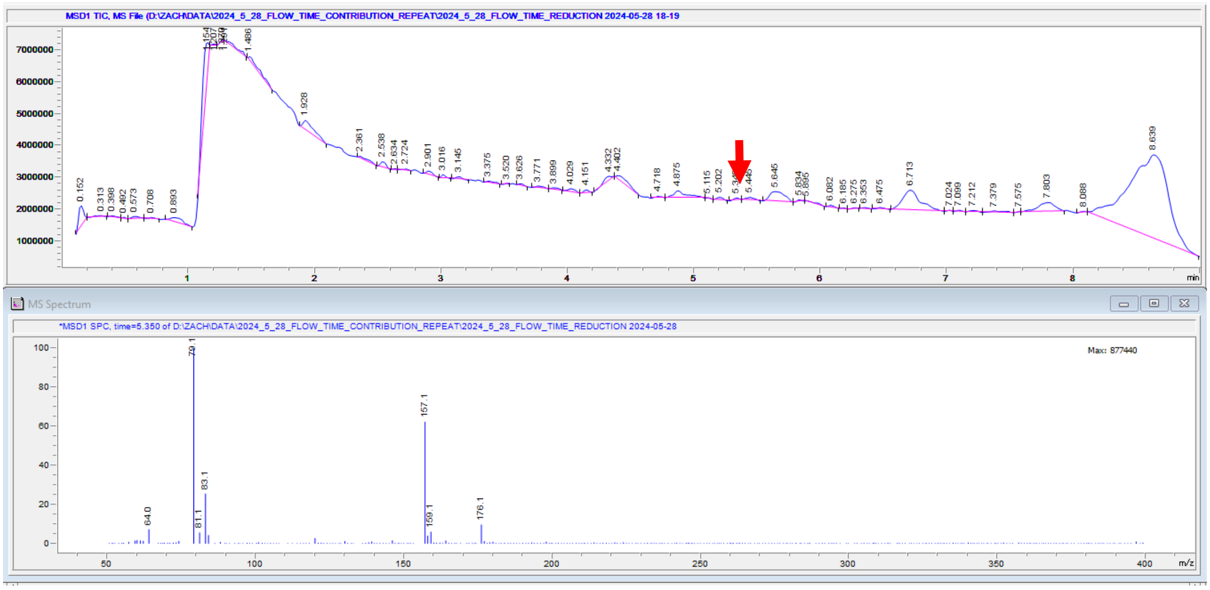

Fig S8.2 (A) ESI-MS fingerprint of the product sample obtained from the flow hydrolysis unit, as to confirm the identities of the IAM and IAA. (A) MS fingerprint of IAM (m/z of 175.1). (B) MS fingerprint of IAA (m/z of 176.1).

S9. Effect of buffer solutions on hydrolysis

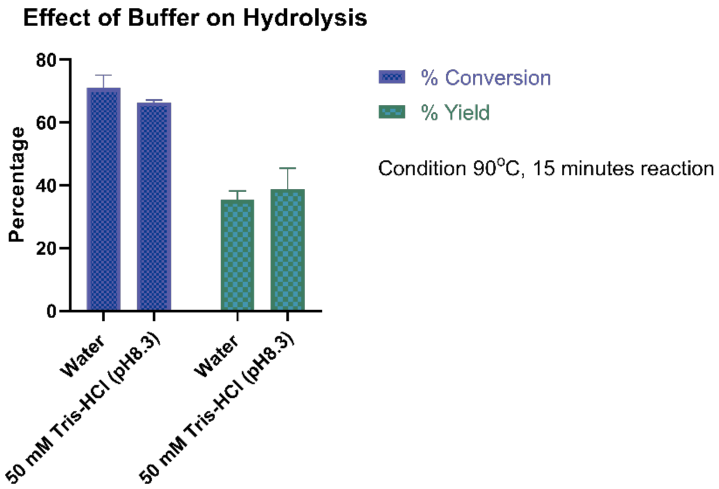

Condition 90°C, 15 minutes reaction

Fig S9. The effect of the buffer (50 mM Tris-HCl buffer, pH 8.3) used in the enzymatic unit on the hydrolysis of IAM at 90 °C conditions.

S10. Proton nuclear magnetic resonance of the standard IAA and isolated IAA

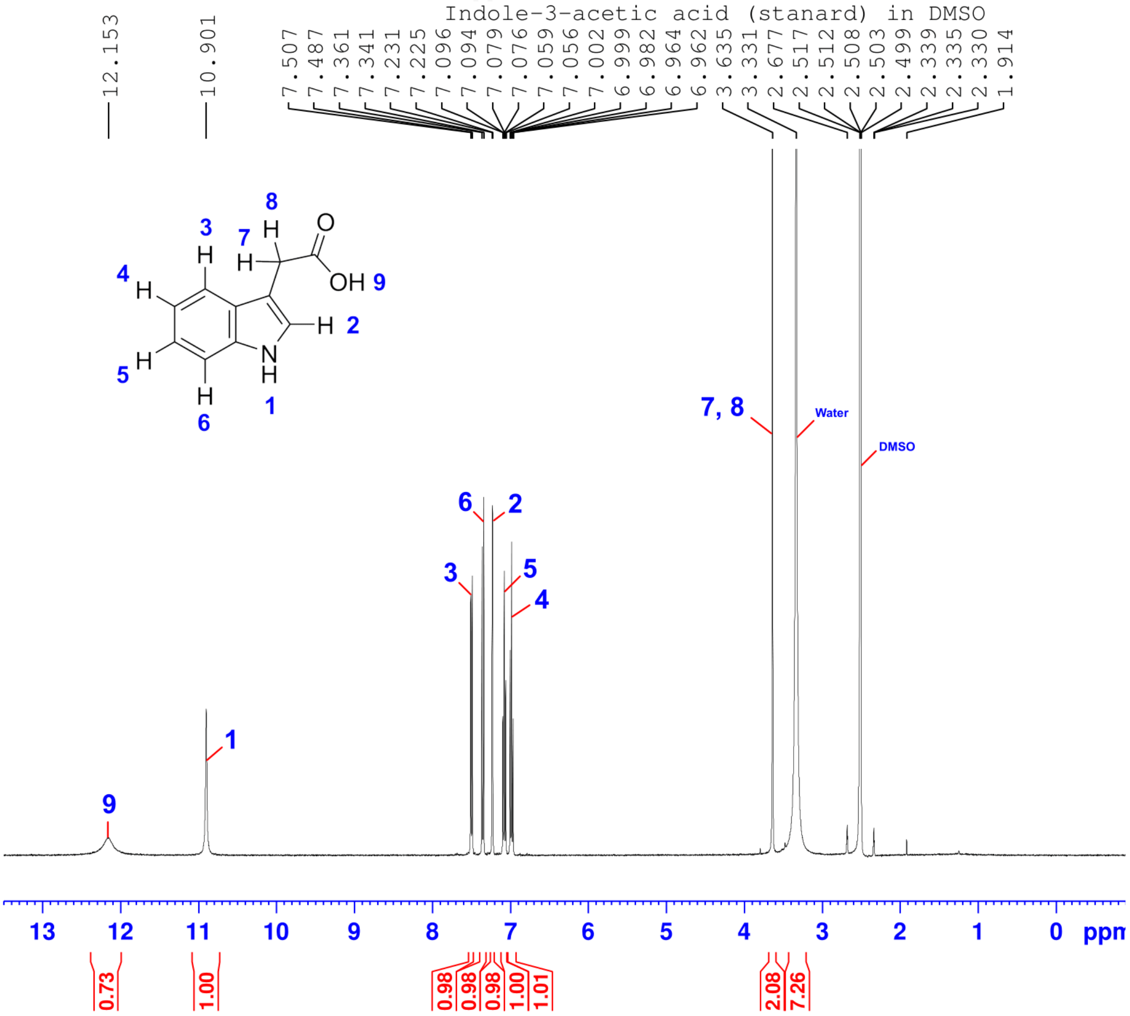

Fig. S10.1 Proton NMR spectrum of indole-3-acetic acid (standard compound): ^{1}H NMR (400 MHz, DMSO-d_6) δ: 12.15 (s, 1H, COOH), 10.90 (s, 1H, NH), 7.50 (d, J = 8.0 Hz, 1H), 7.35 (d, J = 8.0 Hz, 1H), 7.23 (s, 1H), 7.07 (t, J = 6.4 Hz, 1H), 6.98 (t, J =7.0 Hz, 1H), 3.63 (s, 2H); DMSO at 2.50 (solvent), water at 3.33 (trace).

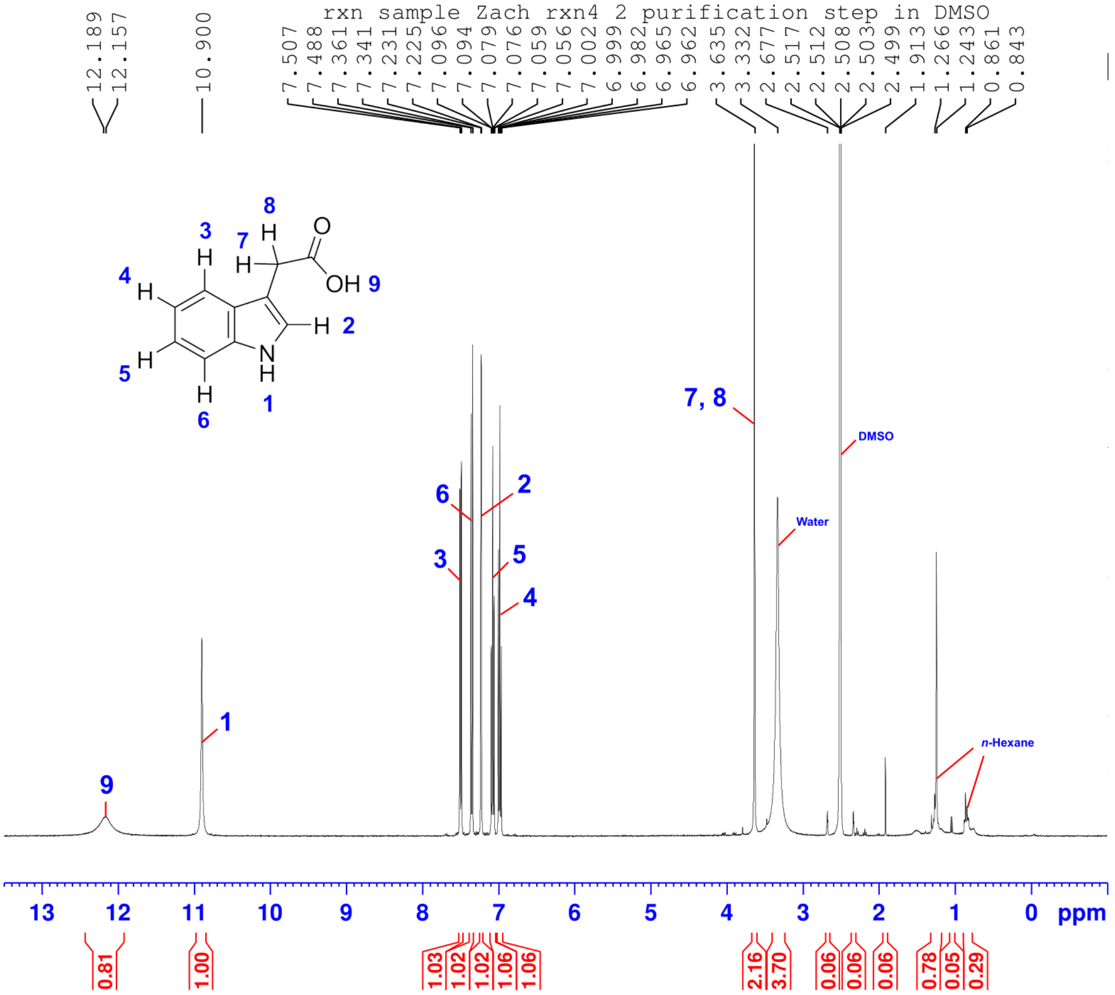

Fig. S10.2 Proton NMR spectrum of the IAA product after isolation (isolated IAA): ^{1}H NMR (400 MHz, DMSO-d_6) δ: 12.17 (s, 1H, COOH), 10.90 (s, 1H, NH), 7.50 (d, $J = 7.6$ Hz, 1H), 7.35 (d, $J = 8.0$ Hz, 1H), 7.23 (s, 1H), 7.08 (t, $J = 6.4$ Hz, 1H), 6.98 (t, $J =6.8$ Hz, 1H), 3.63 (s, 2H); DMSO at 2.50 (solvent), water at 3.33 (trace), *n*-hexane at 0.86 and 1.26, and ethyl acetate at 1.91.

S11. Analytical data of standard compounds

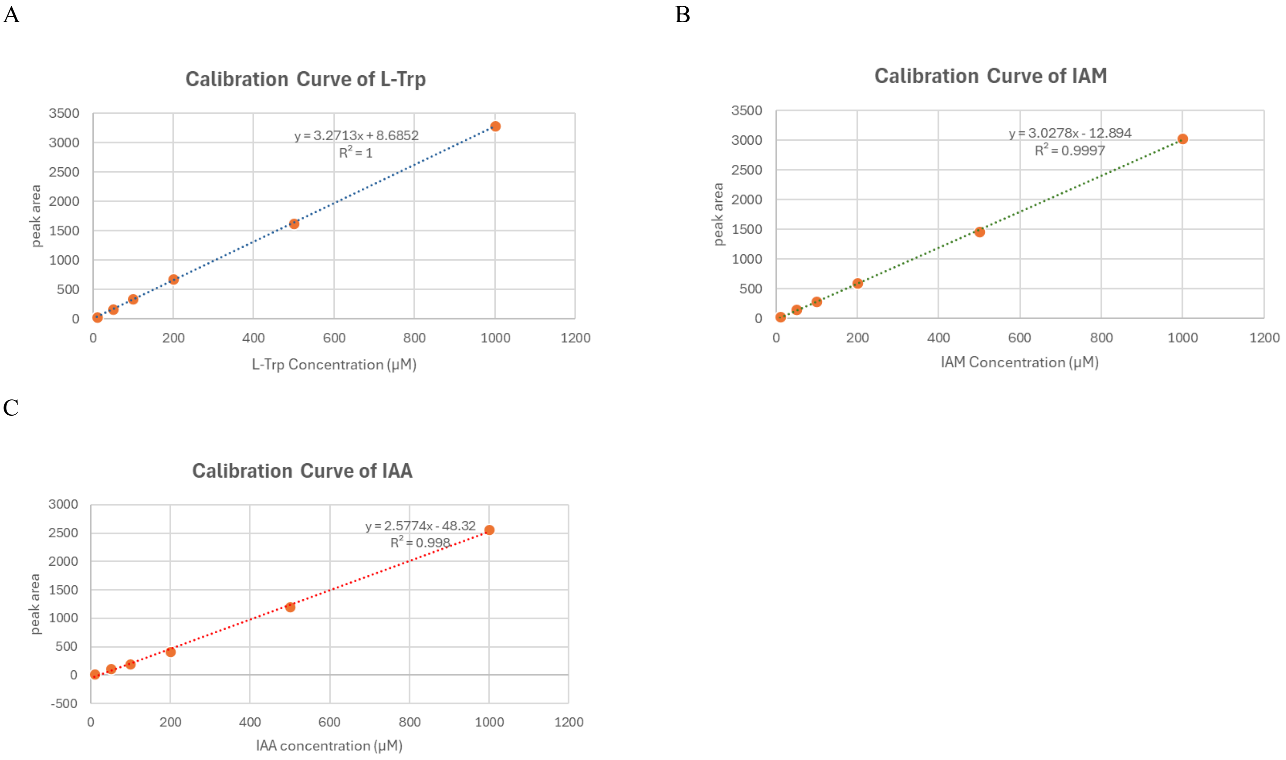

Fig S11.1 Calibration curves obtained from the experimental analysis using HPLC-DAD (A) L-Trp, (B) IAM, (C) IAA.

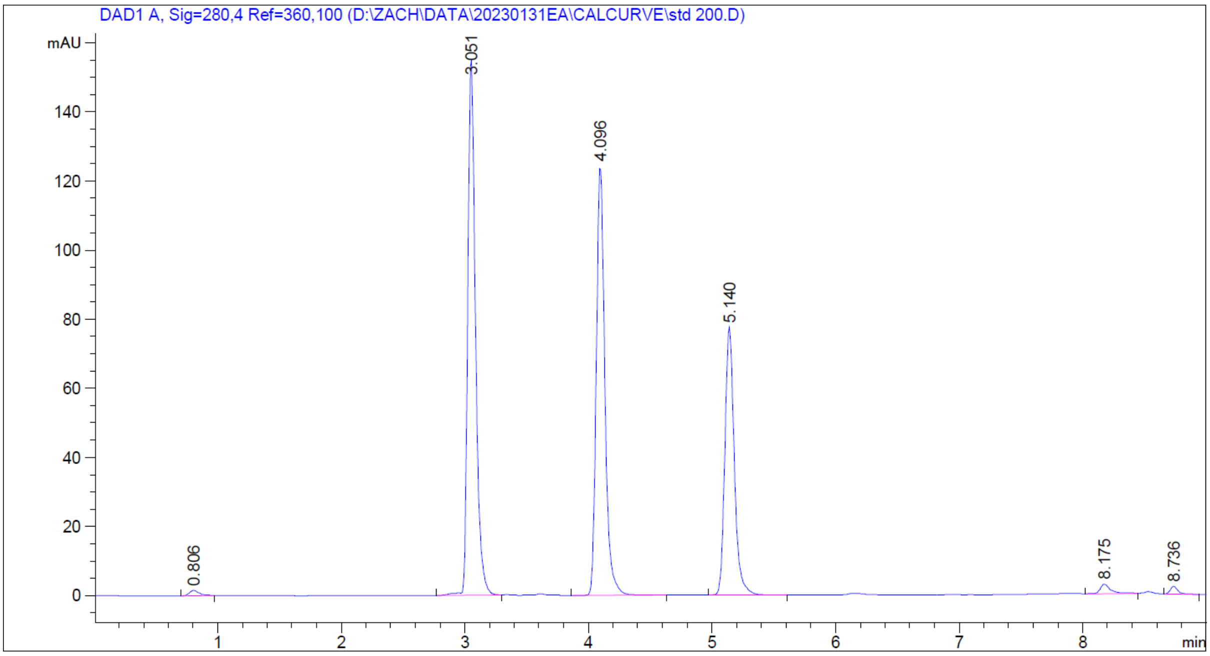

Fig S11.2 The chromatogram of the standard compounds: L-Trp (3.051 min), IAM (4.096 min), and IAA (5.140 min) at a concentration of 200 µM, as analyzed by HPLC-DAD.

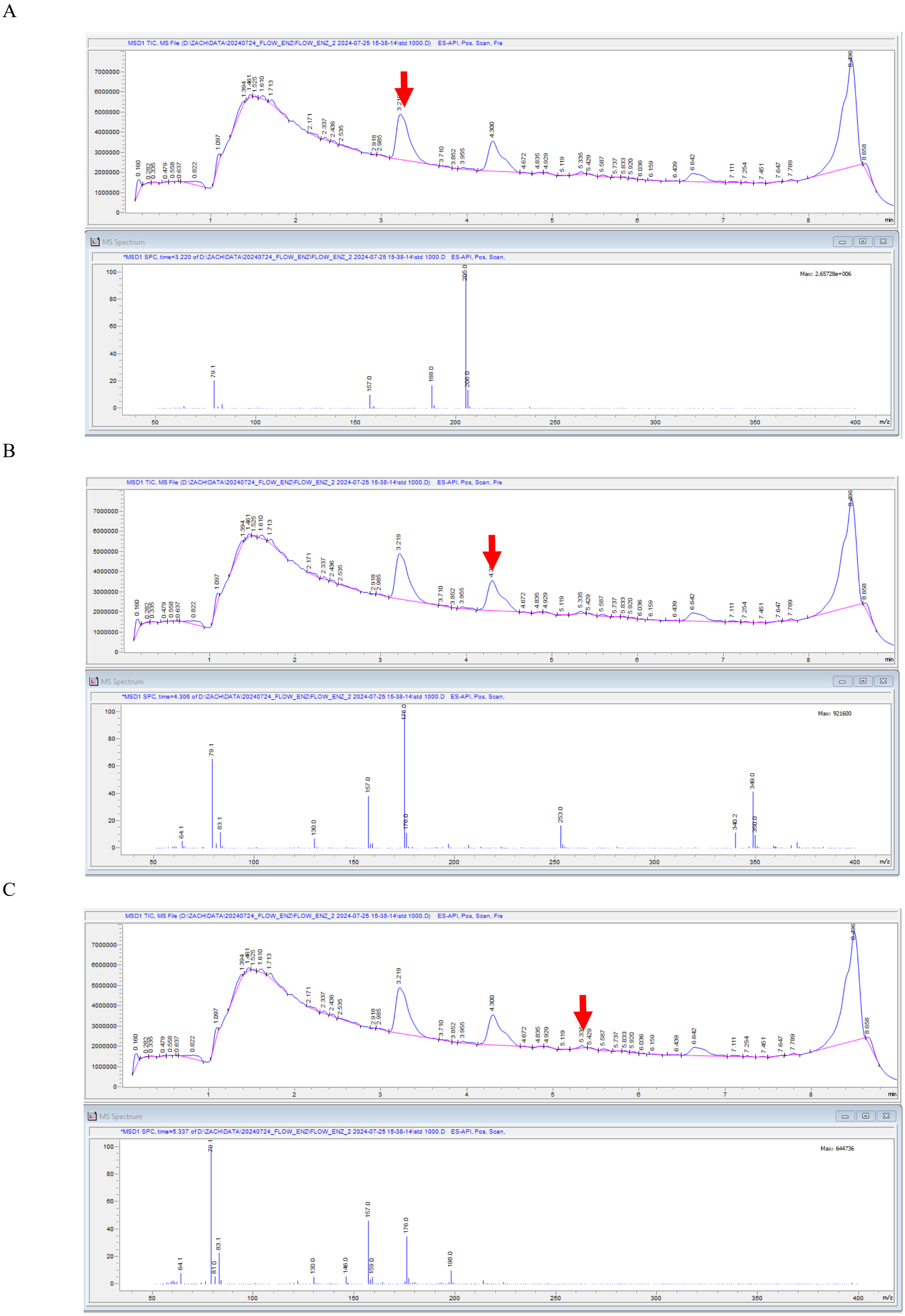

Fig S11.3 Mass spectrometric (MS) fingerprinting of standard compounds using ESI-MS. (A) L-Trp [m/z of 205.0 (*M+1* ion peak), 206.0 (*M+1* isotopic peak)], (B) IAM [m/z of 175.0 (*M+1* ion peak), 176.0 (*M+1* isotopic peak)], and (C) IAA [m/z of 176.0 (*M+1* ion peak)]. The samples were analyzed by HPLC-DAD equipped with a Mass Spectrometer (Agilent Technologies InfinityLab LC/MSD)

List of Notations

w	Mass of catalyst
F_{A0}	Molar flow rate of species A
x	Conversion
$-r'_A$	Specific reaction rate
k'_{cat}	Specific turnover number (nmol.s^{-1}.g$_{cat}^{-1}$)
K_M	Michaelis-Menten constant (µM)
S_0	Initial concentration of substrate in EI-PBR design equation (µM)
Q	Volumetric flow rate (mL.s^{-1}, in EI-PBR)
t	Time
C	Concentration
k	Rate constant
τ	Residence time
STY	Space-time yield (g.L^{-1}.day^{-1})
m_p	Mass of product
V	Volume
$m_{TMO,i}$	Initial mass of TMO
m_b	Mass of bead or support
$Activity_{imTMO}$	Activity of immobilized TMO
$Activity_{freeTMO}$	Activity of free TMO
$Activity_i$	Activity of immobilized TMO at the first cycle
$Activity_n$	Activity of immobilized TMO after nth cycle
$t_{1/2}$	Half time
E_a	Activation energy (J.mol^{-1})
R	Universal gas constant (8.314 J.mol^{-1}.K^{-1})
T	Temperature
A	Frequency factor
h	Characteristic length of reactor
D'_{AB}	Diffusion coefficient in m^2.s^{-1}
D_{AB}	Diffusion coefficient in cm^2.s^{-1}
Φ	Association parameter
M_B	Molecular weight of solvent B (g.mol^{-1})
η_B	Viscosity of solvent B (cP)
V_A	Molar volume of solute A (cm^3.g^{-1}.mol^{-1}.K^{-1})
r	Radius
L	Length
Nu	Nusselt number
T_i	Initial temperature
T_f	Final temperature
b	Thickness of tubing
D_t	Internal diameter
k_t	Thermal conductivity of tubing (W.cm^{-1}.K^{-1})
k_l	Thermal conductivity of liquid (W.cm^{-1}.K^{-1})
h_t	Heat transfer coefficient of tubing
h_l	Heat transfer coefficient of liquid
U	Mean velocity
M	Multiple term
z	Axial position along the tubing
P	Pressure
α, β, γ	Antoine's coefficients